



Hierarchically porous Zr-MOFs labelled methylene blue as signal tags for electrochemical patulin aptasensor based on ZnO nano flower

Baoshan He*, Xiaoze Dong

School of Food Science and Technology, Henan Key Laboratory of Cereal and Oil Food Safety Inspection and Control, Henan University of Technology, Lianhua Road 100#, Zhengzhou High & New Technology Industries Development Zone, Zhengzhou 450001, Henan Province, People's Republic of China

ARTICLE INFO

Keywords:

Electrochemistry
Zr-MOF
PAT
Rapid detection
Aptamer

ABSTRACT

In this work, the feasibility of a novel sensitive electrochemistry aptasensor for the detection of patulin (PAT) using hierarchically porous metal organic framework@methylene blue connection aptamer as signal tags was demonstrated. The substrate electrode of the aptasensor was prepared by electrodeposited gold nanoparticles (AuNPs) on chitosan-zinc oxide nano flower-modified electrode. Subsequently, the complementary single-stranded DNA was attached to the surface of the modified electrode by Au-S bond. Signal tags self-assemble on the surface of modified electrodes by aptamer-cDNA binding, while methylene blue as mediator for electrochemical detection. Thanks to the large specific surface area provided by zinc oxide nano flower, the electrode can load more signal tags and AuNPs to achieve signal amplification. In presence of PAT, Apt preferentially binds to PAT, causing dissociation of some Apt-cDNA and releasing some signal tags leading, resulting in decreased electrical signals. Under optimal conditions, the change in electrochemical signal was proportional to the logarithm of PAT concentration, from 5×10^{-8} – $5 \times 10^{-1} \mu\text{g mL}^{-1}$, and the detection limit was estimated to be $1.46 \times 10^{-8} \mu\text{g mL}^{-1}$. The aptasensor exhibited acceptable reproducibility, renewability, long-term stability and specificity. Moreover, aptasensor was reliable in determination of PAT in spiked apple juice samples.

1. Introduction

Patulin (4-hydroxy-4H-furo[3,2-c]pyran-2(6H)-one, PAT), is a more fatal product of *Penicillium*, *Byssoschlamys* and *Aspergillus* fungus metabolism process [1]. The cytotoxic effect of patulin is ascribed to its interaction with the thiol and amino functional moieties in proteins and amino acids, which may affect the activity of some important enzymes [2]. It has been proved that PAT has carcinogenicity, teratogenicity, mutagenicity, neurotoxicity [3]. PAT is widely present in apples and decaying fruits, and due to its thermal stability and acid resistance, the general food preparation process cannot completely eliminate PAT [4]. Owing to universal toxicity and existence of PAT, many countries and organizations in the world have been established various regulatory protocols for PAT [5]. The United States, Europe and China have established maximum permitted level at $50 \mu\text{g kg}^{-1}$ for PAT in fruit-based products [5,6]. World Health Organization (WHO) together with Food and Agriculture Organization (FAO) has suggested a provisional maximum tolerable daily intake for PAT of $0.4 \mu\text{g kg}^{-1}$ body weight/day [2,6].

Various analytical methods for the identification and quantification of PAT have been developed, such as thin layer chromatography (TLC)

[7], high performance liquid chromatography (HPLC) [8], high-performance liquid chromatography tandem mass spectrometry (HPLC-MS/MS) [9], gas chromatography-mass spectrometry (GC-MS) [10] and colorimetry [11], etc. Some of them are relatively expensive, require large equipment and are cumbersome to operate, which cannot meet the high-throughput testing tasks of the food industry [6]. Moreover, PAT and its artificial antigen have a high degradation rate in animal body, so the development of a commercial kit for PAT detection remains stagnant [1,2]. Currently, electrochemical technique has been received enormous interests, due to its significant virtue of sensitivity, specificity, cost-effectiveness and small target detection [12,13]. In addition, aptamer (Apt) have been widely employed in developing various novel assay methods particularly biosensor platforms [14]. Apt exhibit unique features including higher sensitivity and selectivity to their targets, high stability, controlled synthesis [15]. Therefore, we have developed a study based on aptasensor for PAT detection.

Zinc oxide (ZnO) is a common semiconductor material, and has the advantages of low production cost and non-toxicity [16]. Compared with ZnO nanoparticles, zinc oxide nanoflowers (ZnO NFs) have a larger specific surface area and have relative chemical stability in physiological environment, making them ideal for building sensors

* Corresponding author.

E-mail address: hebaoshan@126.com (B. He).

<https://doi.org/10.1016/j.snb.2019.05.045>

Received 28 March 2019; Received in revised form 26 April 2019; Accepted 14 May 2019

Available online 15 May 2019

0925-4005/ © 2019 Elsevier B.V. All rights reserved.

[17]. Chitosan (CS) is used as a material for immobilizing ZnO NFs to the surface of gold electrode (AuE) because it has effective film-forming properties and adhesion. And it is rich in amino groups, which can provide active sites for further immobilization of gold nanoparticles (AuNPs) [18]. AuNPs have high conductivity, and electrodeposited gold nanoparticles are commonly used to improve the conductivity of electrodes [19]. Moreover, single or multiple layers of gold nanoparticles can serve as an immobilizing matrix for biomolecules [20]. Metal organic framework (MOF) is a porous crystalline material formed by a special metal ion interface and an organic ligand as a linker [21]. UiO-66 is a nanoscale metal organic framework based on Zr (IV) with good electrochemical stability [22]. In addition, because of its adjustable nano size and excellent encapsulation efficiency, it is considered to be an ideal material for the preparation of biochemical assay probes [23]. Hierarchically porous metal organic framework HP-UiO-66 not only has the performance of the traditional UiO-66, but also has a larger pore size, so it can provide the required accessibility to methylene blue (MB) [24]. MB is used as an effective mediator for current sensor preparation due to its low redox potential and good stability [25]. In addition, we hope to synthesize the aminated multilayer metal organic framework HP-UiO-66-NH₂, which is easy to link NH₂-Apt by using glutaraldehyde as a crosslinking agent [26].

Herein, we demonstrate a highly sensitive aptasensor for detecting PAT, obtained by binding hierarchically porous metal organic framework@methylene blue connection aptamer (MOF@MB-Apt) as signal tags to self-assembled complementary single-stranded DNA (cDNA) on the surface of AuNPs-CS-ZnO NFs-modified electrode. For this aptasensor, ZnO NFs provide a large specific surface area for loading more gold nanoparticles and signal tags for signal amplification purposes. MOF is as a carrier for supporting MB and Apt. In the presence of PAT, MOF@MB-Apt signal tags tend to bind to PAT and fall off the surface of the electrode, resulting in a decrease in electrical signal.

2. Experimental

2.1. Materials and reagents

Zinc acetate dihydrate [(CH₃COO)₂Zn·2H₂O] and 2-aminoterephthalic acid (H₂N-BDC) were bought from Alfa Aesar (China) Chemical Co., Ltd. (Shanghai, China). Sodium hydroxide (granules, NaOH) was bought from Luoyang Chemical Reagent Factory (Zhengzhou, China). Cetyltrimethylammonium bromide (CTAB), Lauric acid (Dodecanoic acid), Chitosan (CS), Methylene blue (MB), Tris (2-carboxyethyl) phosphine hydrochloride solution (TCEP), 6-Mercapto-1-hexanol (MCH), Patulin (PAT), Deoxynivalenol (DON), Fumonisin (FB1), Ochratoxin (OTA) and Zearalenone (ZEA) were purchased from Shanghai Yuanye Bio-Technology Co., Ltd. (Shanghai, China). Zirconium tetrachloride (ZrCl₄) was provided by Shandong West Asia Chemical Co., Ltd (Shandong, China). Chloroauric acid (HAuCl₄) was purchased from Aladdin Industrial Co., Ltd (Shanghai, China). Potassium ferrocyanide (K₄Fe(CN)₆·3H₂O) and Potassium ferricyanide (K₃Fe(CN)₆) were bought from Tianjin Guangfu Technology Development Co., Ltd. (Tianjin, China). The functionalized aptamer sequence: 40mer 5'-NH₂-GGCCGCGCAACCGCATCATCTACACTGATATTTTACCTT-3' designed according to a former study [11] and its complementary sequence: 15mer 5'-SH-AAGGTAAATATCAG-3' were purchased from Sangon Biotech Co. Ltd. (Shanghai, China). Tris-HCl (10 mM, pH 7.4, containing 1 mM EDTA) was used as a solvent of Apt. Phosphate buffered saline (PBS; 20 mM, pH 7.4) was prepared with NaCl, Na₂HPO₄ and NaH₂PO₄ solutions. All other chemicals were analytical grade and the double-distilled water was used in all experiments.

2.2. Apparatus

Electrochemical measure was carried out on CHI660E

Electrochemical Workstation (Shanghai CH Instrument Co., China). All samples were studied with X-ray diffraction (XRD, CuK_α radiation, D/max 2550VB X-ray diffractometer, Rigaku, Japan), Fourier transform infrared spectroscopy (FTIR, Bruker, Germany), Scanning electron microscopy (SEM, Hitachi, Japan) and Transmission electron microscope (TEM, HT7700, Hitachi, Japan). Aptasensor was incubated by constant temperature and humidity chamber (Shanghai Yiheng Technology Instrument Co., Ltd., China).

2.3. Preparation of Zinc oxide nano flowers

The preparation of zinc oxide nano flowers (ZnO NFs) was modified based on previous literatures [27]. Briefly, 2 g of zinc acetate was placed in 100 mL of double distilled water, and 8 g of NaOH was slowly placed under magnetic stirring, followed by the addition of 2 g CTAB. The mixed solution was transferred into a hydrothermal reaction kettle in oven at 140 °C for 18 h, centrifuged and dried to obtain ZnO NFs.

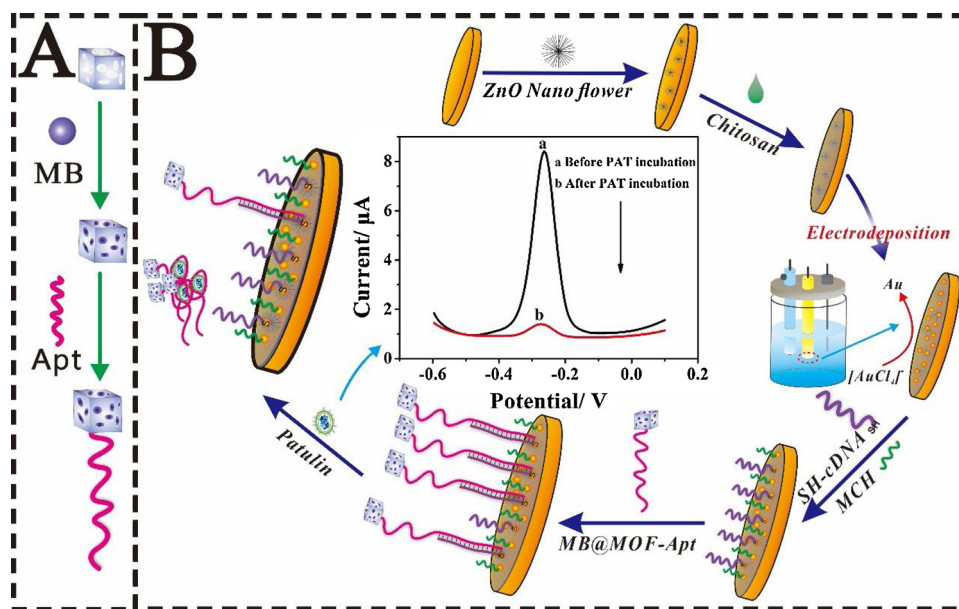
2.4. Preparation of signal tags

The preparation of hierarchically porous metal organic framework@methylene blue labeled aptamer (MB@MOF-Apt) was mostly based on this reported literature [22] and the MOF was prepared with the molar ratio of Zr/BDC/dodecanoic acid = 1/0.5/35. First, ZrCl₄ (320 mg, 1.372 mmol) and excess dodecanoic acid (9.6 g, 48 nmol) were dissolved in 80 mL of DMF and then ultrasonically mixed for 30 min. Subsequently, add H₂N-H₂BDC and continue ultrasonicated for 5 min. The mixed solution was transferred into a hydrothermal reaction kettle in oven at 120 °C for 48 h, centrifuged and dried to obtain yellow powder. The powder sample was washed several times with DMF and then washed with ethanol several times, and finally dried at 120 °C for 12 h to obtain HP-UiO-66-NH₂. Conventional UiO-66-NH₂ was prepared by dissolving the mixture of ZrCl₄ (320 mg, 0.343 mmol) S6 and BDC-NH₂ (248 mg, 0.343 mmol) in DMF (80 mL). Subsequent preparation was consistent with HP-UiO-66-NH₂.

The synthesis of signal tags draws on previous literature [24]. First, dispersed 24 mg of HP-UiO-66-NH₂ (Replace the control group with UiO-66-NH₂) in 8 mL of MB (1 mM) and mixed for 24 h using thermostatic oscillator. The resulting conjugates were centrifuged and then washed with PBS several times to remove the physically adsorbed MB. The product (MOF@MB) was dispersed in 5 mL PBS (pH 7.4) containing 2.5% glutaraldehyde and gently stirred for 2 h. After that, the product was centrifuged and washed several times with PBS. Then, it was incubated with 24 μL of amino-functionalized aptamer (NH₂-Apt, 10 mM) for 2 h, centrifuged to remove unadsorbed aptamer, and the conjugate was dispersed in 2.4 mL of PBS. The MB@MOF-Apt was kept at 4 °C before use. The schematic diagram of the MB@MOF-Apt signal tags is shown in Scheme 1 A.

2.5. Preparation of aptasensor

The construction and principle of the patulin aptasensor is illustrated in Scheme 1 B. AuE was pretreated with alumina powder, then washed with ethanol and deionized water, and activated in a piranha etching solution (H₂SO₄: H₂O₂ = 7:3, V/V) for 30 min. The 3.0 μL ZnO NFs suspension (1 mg mL⁻¹) was applied on AuE, and after drying, CS (1 mg mL⁻¹, contain 2.4 μL mL⁻¹ glacial acetic acid) was dropped and continue to dry to prepare CS-ZnO NFs/AuE. ZnO NFs on the surface of the electrode can effectively increase the loading of the Au NPs and signal tags, and maintain the relatively stable microenvironment, thereby improving the electrode detection performance. CS can not only attach ZnO NFs to the AuE surface, but also can provide active sites for further AuNPs immobilization because the rich amino groups of CS. Then, AuNPs was immobilized by electrodeposition [19]. The electrode was immersed in HAuCl₄ (10 mM) for 40 min and then electrochemically reduced in PBS for 10 min at -0.8 V to anchor AuNPs to the



Scheme 1. Schematic diagram:(A) MB@MOF-Apt signal tags and (B) Aptasensor to detect PAT.

surface of CS-ZnO NFs/AuE. Loading of AuNPs will greatly improve electrode performance. After cleaning the electrode with PBS, 3 μ L of thiol-labeled cDNA (SH-cDNA, 2 mM, contain 10 mM TrisHCl, 1 mM EDTA, pH = 7.4) was dropwise added onto the surface of AuNPs/CS-ZnO NFs/AuE and incubated for 120 min. The SH-cDNA can be immobilized on the surface of AuNPs/CS-ZnO NFs/AuE by Au-S bond. After the electrode was washed with Tris-HCl, 3 μ L of 1 mM MCH was added for 30 min to prevent nonspecific adsorption. The surface of AuE was rinsed thoroughly with Tris-HCl (0.1 M) buffer to obtain MCH/cDNA/AuNPs/CS-ZnO NFs/AuE. Subsequently, 10 μ L of the prepared MB@MOF-Apt signal tags were coated and incubated for 100 min. The load of the signal tags was attributed to the binding of the Apt-cDNA. And then the MB@MOF-Apt/MCH/cDNA/AuNPs/CS-ZnO NFs/AuE was washed with Tris-HCl and kept at 4 $^{\circ}$ C before use.

2.6. Aptasensor detection of PAT

Dilute PAT to a series of concentrations (5×10^{-1} – 5×10^{-8} μ g mL $^{-1}$) using PBS. 5 μ L of desired concentration PAT was added to the surface of the modified electrode (MB@MOF-Apt/MCH/cDNA/AuNPs/CS-ZnO NFs/AuE) and then incubated for 40 min. Subsequently, it was washed with Tris-HCl and then performed Electrochemical Impedance Spectroscopy (EIS) and Differential Pulse Voltammetry (DPV) detection.

The experimental principle was based on the fact that after PAT incubation, the Apt preferentially binds to PAT, causing dissociation of some Apt-cDNA and releasing some MB@MOF-Apt signal tags. The concentration of PAT was quantified according to the value of peak current change (ΔI). The ΔI calculation formula: $\Delta I = I_0 - I_1$, where I_0 is peak DPV current value before incubation of PAT, I_1 is peak DPV current value after incubation of PAT. And the peak voltage is -0.264 V (vs. Saturated calomel electrode). EIS was tested in 5 mM [Fe(CN) $_6$] $^{3-4-}$ solution including 0.1 M KCl at signal amplitude of 5 mV in the frequency range of 10 kHz to 10 mHz. DPV was performed in PBS with a potential range from -0.6 V to 0.1 V and the parameters applied were the following: 50 mV pulse amplitude, 0.05 pulse width, and 0.5 s pulse period. CV was tested in 5 mM [Fe(CN) $_6$] $^{3-4-}$ solution including 0.1 M KCl at sweep speed of 0.1 V s $^{-1}$. Constant temperature and humidity chamber parameter setting: 37 $^{\circ}$ C temperature, 80% humidity.

3. Results and discussion

3.1. Characterization of materials

XRD confirmed the successful synthesis of the ZnO NFs. As shown in Fig. 1, the thumbnail is XRD standard pattern of ZnO, all diffraction peaks exactly match the XRD standard pattern of ZnO. No other additional diffraction peaks from impurities are observed, implying the high purity of all the samples. And the XRD pattern of ZnO NFs was consistent with the reported literature results [28,29]. Also, we used SEM to characterize ZnO NFs, as Fig. 1 (B) shows. SEM image of ZnO NFs clearly shows the typical nanoflower morphology with a diameter of 20 μ m, which was composed of nanoneedles.

The prepared MOF(HP-UiO-66-NH $_2$ and UiO-66-NH $_2$) structure was recorded by XRD and FTIR spectra. The XRD obtained for the as-synthesized samples are reported in Fig. 1 (C) and reveal that the materials are indeed crystalline. All diffraction peaks of HP-UiO-66-NH $_2$ and UiO-66-NH $_2$ were consistent, indicating that HP-UiO-66-NH $_2$ is topologically equivalent with UiO-66-NH $_2$. This result is consistent with the reported literature [24,26]. As shown in Fig. 1 (D), the FTIR spectroscopy shows that UiO-66-NH $_2$ and HP-UiO-66-NH $_2$ structures are similar, while the characteristic vibrational bands of the free -NH $_2$ group of the UiO-66-NH $_2$ appears at 3340 and 3469 cm $^{-1}$ and HP-UiO-66-NH $_2$ appears at 3360 and 3468 cm $^{-1}$, which was the key to our preparation of signal tags. This result is consistent with the reported literature [30,31]. TEM and SEM further validated the success of HP-UiO-66-NH $_2$. By comparing TEM of UiO-66-NH $_2$ [Fig. 1 (E)] and TEM of HP-UiO-66-NH $_2$ [Fig. 1 (F)], it is clear that HP-UiO-66-NH $_2$ has good dispersion and larger particle diameter (\approx 70 nm). Further comparison of SEM of UiO-66-NH $_2$ [Fig. 1 (G)] and SEM of HP-UiO-66-NH $_2$ [Fig. 1 (H)] confirmed that HP-UiO-66-NH $_2$ has larger particle diameter and is more uniform in size. These results indicate that we have successfully prepared HP-UiO-66-NH $_2$ with larger particle size and uniformity than traditional UiO-66-NH $_2$.

3.2. Electrochemical characterization of prepared aptasensor

The EIS spectrum consists of a semicircle at high frequencies and straight line at low frequencies, where the semicircular portion at high frequencies corresponds to the charge transfer limiting process and the linear portion at low frequencies corresponds to the diffusion limiting

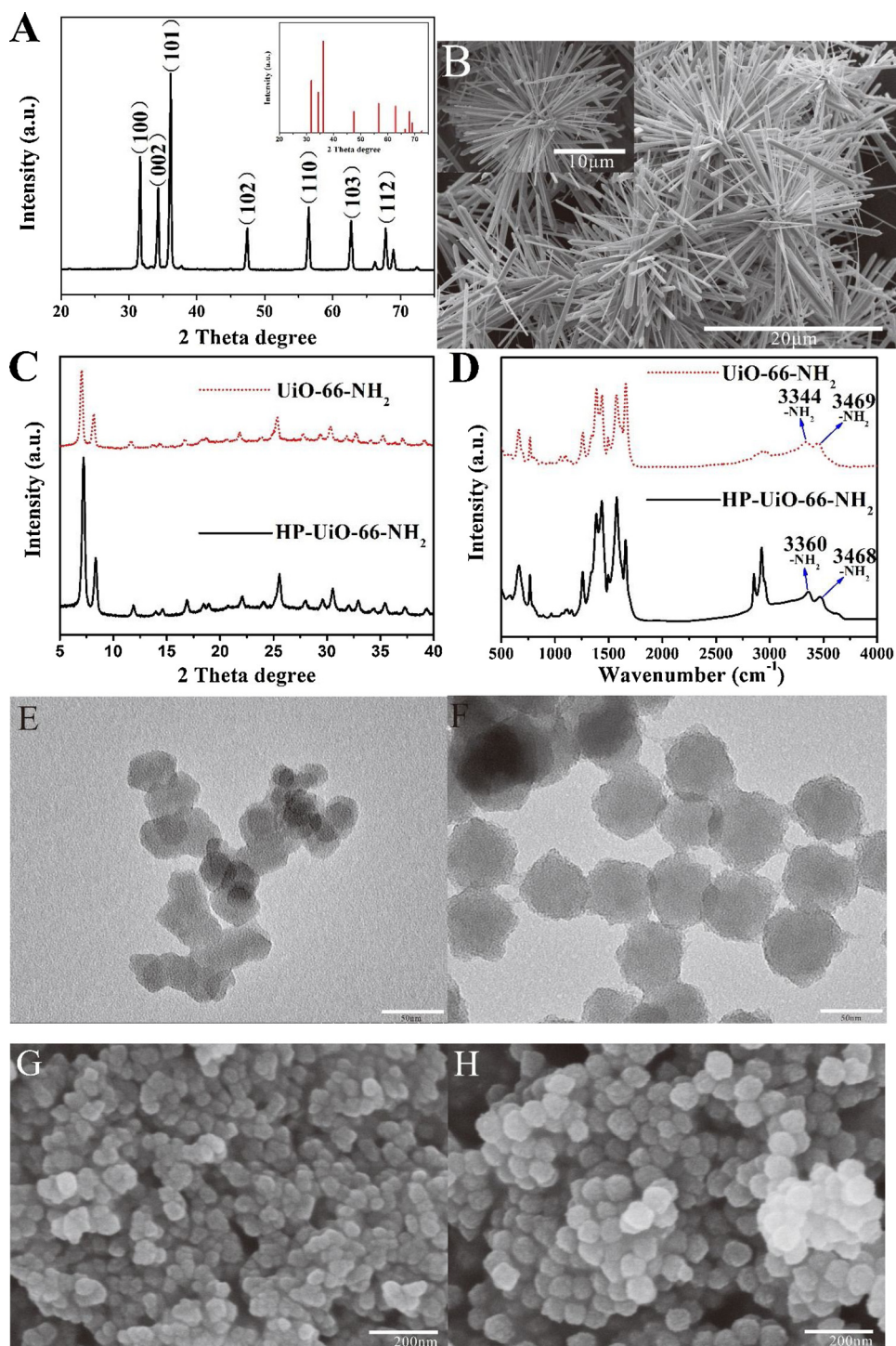


Fig. 1. A)XRD pattern of ZnO NFs, (B)SEM image of ZnO NFs, (C)XRD pattern of UiO-66-NH₂ and HP-UiO-66-NH₂, (D)FTIR spectra of UiO-66-NH₂ and HP-UiO-66-NH₂, (E)TEM image of UiO-66-NH₂, (F) TEM image of HP-UiO-66-NH₂, (G) SEM image of UiO-66-NH₂ and (H) SEM image of HP-UiO-66-NH₂.

process. Fig. 2 shows the EIS characterization results of each immobilization step. Thus, the value of the electron transfer resistance is obtained by measuring the diameter of the semicircle. It can be seen that bare AuE shows a relatively small semicircle in the Nyquist diagram of the impedance spectrum, and the electron transfer resistance (Ret) was 101 Ω (curve a) fitted to the equivalent circuit R(C(RW))(inset in Fig. 2). After adding ZnO NFs dropwise and fixing with CS, the conductivity of ZnO NFs is poor, resulting in the value of Ret increased to 335 Ω (curve b). Based on the large specific surface area provided by ZnO NFs and the adsorption properties of the amino-rich CS, a large

amount of AuNPs were deposited on the surface of the electrode after electrodeposition, which causes Ret was obviously declined to 30 Ω (curve c). When the SH-cDNA was covalently immobilized on the surface of AuNPs/CS-ZnO NFs/AuE by the Au-S bond, Ret was increased to 260 Ω (curve d). This is due to electrostatic repulsion between the negatively charged phosphate group of the cDNA and the negatively charged redox probe [Fe(CN)₆]^{3-/4-}. In order to cover the non-specific sites on the surface of the modified electrode, the cDNA/AuNPs/CS-ZnO NFs/AuE should be incubated with MCH, which further increases Ret to 485 Ω (curve e). Subsequently, the drop of MB@MOF-Apt signal tags to

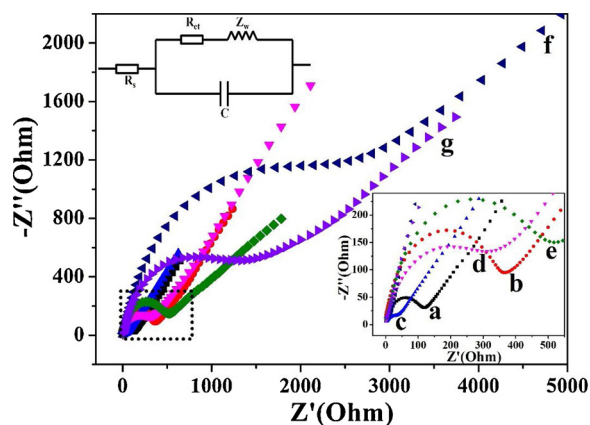


Fig. 2. EIS of each immobilization step: (a) bare AuE, (b) CS-ZnO NFs/AuE, (c) AuNPs/CS-ZnO NFs/AuE, (d) cDNA/AuNPs/CS-ZnO NFs/AuE, (e) MCH/cDNA/AuNPs/CS-ZnO NFs/AuE, (f) MB@MOF-Apt/MCH/cDNA/AuNPs/CS-ZnO NFs/AuE, and (g) PAT ($5 \times 10^{-3} \mu\text{g mL}^{-1}$)/MB@MOF-Apt/MCH/cDNA/AuNPs/CS-ZnO NFs/AuE. Inset is the R(C(RW)) equivalent circuit model, which included the solution resistance (R_s), double layer capacitance (C), warburg impedance (Z_w), and electron transfer resistance (R_{ct}).

the surface of MCH/cDNA/AuNPs/CS-ZnO NFs/AuE causes a significant increase in R_{ct} value to 2000Ω (curve f), mainly due to the poor conductivity of the MOF and the phosphate group of the Apt. Finally, the MB@MOF-Apt/MCH/cDNA/AuNPs/CS-ZnO NFs/AuE was used to capture PAT. The R_{ct} decreased to 1172Ω (curve g) after the Apt specifically capturing the $5 \times 10^{-3} \mu\text{g mL}^{-1}$ of PAT. This is due to the fact that Apt preferentially binds to PAT, causing some dissociation of Apt-cDNA and releasing some MB@MOF-Apt. The results all above reflect that the fabrication procedures were successful and the proposed aptasensor was suitable for PAT detection.

Moreover, DPV was employed to study the amplification effect of the prepared ZnO NFs on the performance of the modified electrode. As shown in Fig.S1(A), curves a and b represent DPV measurements of MOF-Apt/MCH/cDNA/AuNPs/CS-ZnO NFs/AuE and MOF-Apt/MCH/cDNA/AuNPs/CS/AuE, respectively. By measuring the signal of MB after incubation of MB@MOF-Apt signal tags, it can be seen that the peak current value increases by about 40% after the ZnO NFs modified electrode. This indicates that ZnO NFs can increase the specific surface area of the electrode and thereby increase the loading of the AuNPs and signal tags. Fig.S1(B) shows that HP-UiO-66-NH₂ can load more methylene blue than conventional UiO-66-NH₂, and the DPV signal is increased by 53%. Fig.S1(C) shows the change in DPV curve after incubating MB@MOF-Apt/MCH/cDNA/AuNPs/CS-ZnO NFs/AuE with $5 \times 10^{-3} \mu\text{g mL}^{-1}$ PAT. When MB@MOF-Apt and PAT performs the recognition reaction, the peak current value was significantly reduced ((curve a to curve b). DPV measurement results are consistent with EIS results, indicating that DPV can be successfully applied to detect PAT. As shown in Fig.S1(D) curves a, b and c represent CV (Inset is EIS) measurements of AuE, AuNPs/CS/AuE and AuNPs/CS-ZnO NFs/AuE, respectively. According to the Randles-Sevcik equation [32]: $I_p = 2.69 \times 10^5 n^{3/2} A D^{1/2} v^{1/2} C_0$. In this experiment, n is 1 (number of electron transfer), D is $6.7 \times 10^{-6} \text{cm}^2 \text{s}^{-1}$ (diffusion coefficient), C_0 is 5 mM (potassium ferricyanide concentration), and v is 0.1V s^{-1} (sweep speed). Calculated that the active area of AuE is $0.125(\text{cm}^2)$, AuNPs/CS/AuE is $0.143(\text{cm}^2)$, AuNPs/CS-ZnO NFs/AuE is $0.155(\text{cm}^2)$. This result indicates that ZnO NFs can increase the surface area of the electrode, thereby increase the current.

3.3. Optimization of detection conditions

In order to achieve the best electrode detection performance, we have carefully optimized some parameters. We optimized three

parameters including ZnO NFs volume, cDNA concentration and MB@MOF-Apt signal tags incubation time by detecting the peak current after MB@MOF-Apt signal tags incubation. Then the parameter PAT interaction time was optimized by detecting the ΔI value after $5 \times 10^{-3} \mu\text{g mL}^{-1}$ PAT incubation.

From Fig.S2 (A), the peak current increased significantly as the volume of ZnO NFs added increased from $0 \mu\text{L}$ to $3 \mu\text{L}$. Subsequently, the addition of ZnO NFs from $3 \mu\text{L}$ to $5 \mu\text{L}$ causes the peak current to gradually decrease. This is because ZnO NFs provides more binding sites for loading more AuNPs and MB@MOF-Apt signal tags, but ZnO NFs is poorly conductive, and excessive ZnO NFs causes the current value to begin to decrease. Therefore, $3 \mu\text{L}$ was set as the optimal volume of ZnO NFs.

The amount of cDNA modification was studied by adding $3 \mu\text{L}$ cDNA with concentrations of $0.5 \mu\text{M}$ – $3 \mu\text{M}$. As shown in Fig.S2 (B), the peak current increased with the concentration of cDNA ranging from 0.5 to $2.0 \mu\text{M}$, and then it started to remain relatively constant at much higher concentration. This may be due to the limited amount of cDNA loaded on the prepared electrode. In order to prevent unnecessary waste, we chose the $2 \mu\text{M}$ cDNA as optimal titration concentration.

Optimization of the incubation time of the MB@MOF-Apt signal tags is shown in Fig.S2 (C). By comparing the strength of the peak signal, it was found that the peak current remarkably increased with the incubation time increased from 40 min to 100 min and then stabilized after 100 min , probably because the MB@MOF-Apt signal tags incubation was almost completed at 100 min . Therefore, 100 min was chosen as the best MB@MOF-Apt signal tags incubation time for further testing.

Additionally, the incubation time of the target toxin $5 \times 10^{-3} \mu\text{g mL}^{-1}$ PAT was studied and the results are shown in Fig.S2 (D). Different interaction time of PAT may cause the response current to decline to different extents. Taking into account the analysis time and by comparing the value of ΔI , it can be seen that the best detection was when the incubation time was 40 min .

3.4. Determination of PAT

An aptasensor was constructed using the optimized conditions and used for the detection of PAT. As shown in Fig. 3, MB@MOF-Apt/MCH/cDNA/AuNPs/CS-ZnO NFs/AuE were incubated with 5×10^{-8} , 5×10^{-7} , 5×10^{-6} , 5×10^{-5} , 5×10^{-4} , 5×10^{-3} , 5×10^{-2} and $5 \times 10^{-1} \mu\text{g mL}^{-1}$ PAT, respectively. As shown in Fig.3 (A), the ΔI value gradually increases as the PAT concentration increases. Fig.3 (B) illustrates the ΔI value varied proportionally with logarithmic concentration of PAT from 5×10^{-8} – $5 \times 10^{-1} \mu\text{g mL}^{-1}$. The calibration curve was determined as: $\Delta I(\mu\text{A}) = 0.841 \text{gc}_{\text{PAT}}(\mu\text{g mL}^{-1}) + 7.10$ ($R^2 = 0.997$), and the low detection limit estimated according to the IUPAC method [33] was $1.46 \times 10^{-8} \mu\text{g mL}^{-1}$ (Detailed calculation process in the “Electronic Supplementary Material” file-S1). A comparison between the analytical parameters of some methods for determination of PAT was made, as displayed in Table 1 [1,2,6,11,34,35]. It can be seen that the present aptasensor showed wider linear range and lower detection limit.

3.5. Reproducibility, renewability and long-term stability

The reproducibility of the proposed aptasensor was investigated by six different aptasensors fabricated in the same way. The relative standard deviation (RSD) is 3.47% . On the other hand, the aptasensor achieves renewable by simply re-adding MB@MOF-Apt signal tags. When the second renewable, the DPV response was 93.4% of the original response. When the third renewable, the DPV response was 88.3% of the original value. These results indicated that the prepared electrode can be renewable twice under the premise of ensuring its detection ability. Moreover, the long-term stability of the aptasensor was assayed at 4°C and measured after 10 days . The DPV response was 92.7% of original response, indicating the acceptable long-term stability of the

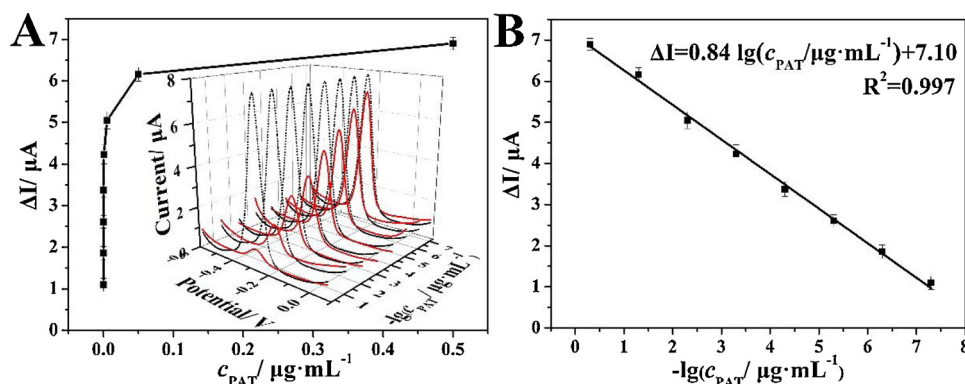


Fig. 3. (A) DPV response diagram of MB@MOF-Apt/MCH/cDNA/AuNPs/CS-ZnO NFs/AuE with PAT concentration in the range of 5×10^{-8} – 5×10^{-1} $\mu\text{g mL}^{-1}$. (B) Calibration curve of ΔI and $-\lg[\text{PAT}]$.

aptasensor. Detailed DPV data graph was shown in Fig.S3. The experimental analysis results were obtained by prepared aptasensor detection of 5×10^{-3} $\mu\text{g mL}^{-1}$ PAT.

3.6. Specificity

Control experiments were performed to characterize the specificity of the proposed aptasensor. As shown in Fig. 4, only 5 ng mL^{-1} PAT and Mixture (contains PAT, DON, AFT, FB1, OTA and ZEA) induced a prominent DPV response change, whereas no significant DPV response change of the aptasensor was observed upon addition of DON (50 ng mL^{-1}), AFT (50 ng mL^{-1}), FB1 (50 ng mL^{-1}), OTA (50 ng mL^{-1}), ZEA (50 ng mL^{-1}). These results indicated the aptasensor have good specificity for PAT detection.

3.7. Detection of PAT in real samples

To assess the applicability of the proposed aptasensor, we applied the prepared aptasensors for PAT detection in apple juice samples (purchased from local supermarkets). 2 mL apple juice samples was added to centrifuge tube and extracted twice with 2 mL of ethyl acetate to remove carbohydrates, proteins, etc. in matrix. Sample of the ethyl acetate layer was collected for drying, and then dispersed in 1 mL PBS. PAT was added to the desired concentration (5×10^{-3} , 5×10^{-5} , 5×10^{-7} $\mu\text{g mL}^{-1}$). The detection results displayed in Table S1 show that the recovery rate was from 92.2–96.8%. This indicates that the prepared aptasensor is feasible to detect PAT in real samples.

4. Conclusions

In summary, we constructed an aptasensor for ultrasensitive detection of PAT using ZnO NFs and MB@MOF-Apt signal tags. This design was based on the large specific surface area provided by ZnO NFs and the large amount of MB mediator carried by MOF. And the PAT concentration was determined by the change of the peak current after PAT incubation. The change of peak current after patulin incubation was measured by DPV to achieve the purpose of detection. The

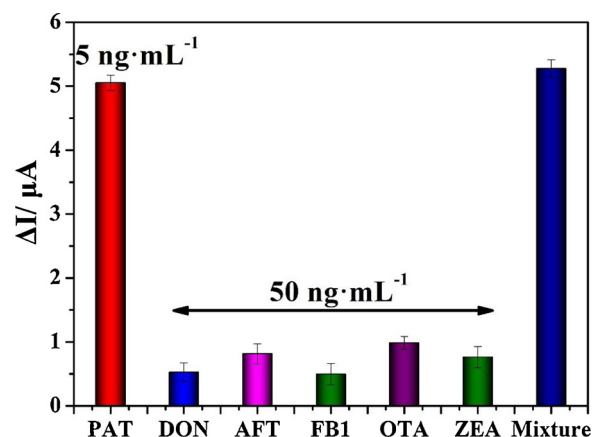


Fig. 4. Specificity evaluation of the proposed aptamer sensor by DPV response for PAT (5 ng mL^{-1}), DON (50 ng mL^{-1}), AFT (50 ng mL^{-1}), FB1 (50 ng mL^{-1}), OTA (50 ng mL^{-1}), ZEA (50 ng mL^{-1}) and Mixture.

aptasensor shows good performance when used to detect PAT, with a wide linear range, low detection limit, reproducibility, renewability, long-term stability and good specificity. Furthermore, the aptasensor was successfully applied to detect PAT in apple juice samples with the recovery rate was 92.2–96.8%. Therefore, based on its excellent performance, it can be a powerful tool for point-of-care detection in the future.

Compliance with ethical standards

The author(s) declare that they have no competing interests.

Acknowledgments

This work was supported by the National Natural Science Foundation of China (Grant No. 61301037), the Cultivation Plan for Young Core Teachers in Universities of Henan Province (No.

Table 1

Comparisons of this work with the other modified electrodes methods for the determination of PAT.

Method	Linear range	detection limit	References
Molecular imprinting (AgNPs@ZnMOF)	0.1–10 $\mu\text{mol L}^{-1}$	0.06 $\mu\text{mol L}^{-1}$	(1)
Molecular imprinting (carbon dots, chitosan, gold nanoparticles)	1×10^{-12} – 1×10^{-9} mol L^{-1}	7.57×10^{-13} mol L^{-1}	(2)
Colorimetric (FRET)	0.01–100 ng mL^{-1}	0.003 ng mL^{-1}	(6)
Colorimetric (aptamer)	50–2500 pg mL^{-1}	48 pg mL^{-1}	(11)
Molecular imprinting (Mn-doped ZnS quantum dots)	0.43–6.50 $\mu\text{mol L}^{-1}$	0.32 $\mu\text{mol L}^{-1}$	(34)
Molecularly imprinted sol-gel polymer	7.5×10^{-3} – 6×10^{-2} $\mu\text{g mL}^{-1}$	3.1×10^{-3} $\mu\text{g mL}^{-1}$	(35)
Aptasensor(MB@MOF-Apt/MCH/cDNA/AuNPs/CS-ZnO NFs/AuE)	5×10^{-8} – 5×10^{-1} $\mu\text{g mL}^{-1}$	1.46×10^{-8} $\mu\text{g mL}^{-1}$	This work

2017GGJS072), the Henan Science and Technology Cooperation Project (Grant No. 172106000014), the Youth Backbone Teacher Training Program of Henan University of Technology (Grant No. 21420004), and the National Engineering Laboratory for Wheat & Corn Further Processing, Henan University of Technology (No. NL2018004).

Appendix A. Supplementary data

Supplementary material related to this article can be found, in the online version, at doi:<https://doi.org/10.1016/j.snb.2019.05.045>.

References

- [1] N. Bagheri, A. Khataee, B. Habibi, J. Hassanzadeh, Mimetic ag nanoparticle/zn-based mof nanocomposite (agnps@znmof) capped with molecularly imprinted polymer for the selective detection of patulin, *Talanta* 179 (2018) 710–718.
- [2] W. Guo, F. Pi, H. Zhang, J. Sun, Y. Zhang, X. Sun, A novel molecularly imprinted electrochemical sensor modified with carbon dots, chitosan, gold nanoparticles for the determination of patulin, *Biosens. Bioelectron.* 98 (2017) 299–304.
- [3] E. Diao, D. Ren, T. Liu, J. Zhang, W. Hu, Ozone detoxification of patulin in aqueous solution and cytotoxic evaluation using human hepatic carcinoma cells, *Toxicol.* 155 (2018) 21–26.
- [4] X. Li, H. Li, X. Li, Q. Zhang, Determination of trace patulin in apple-based food matrices, *Food Chem.* 233 (2017) 290–301.
- [5] A.K.E. Aytunga, Adsorptive recovery of phenolics from apple juice via batch and fixed bed column, *J. Food Eng.* 239 (2018) 114–121.
- [6] Z. Wu, E. Xu, Z. Jin, J. Irudayaraj, An ultrasensitive aptasensor based on fluorescent resonant energy transfer and exonuclease-assisted target recycling for patulin detection, *Food Chem.* 249 (2018) 136–142.
- [7] J.E. Welke, M. Hoeltz, H. A. H. Dottori, I.B. Noll, Quantitative analysis of patulin in apple juice by thin-layer chromatography using a charge coupled device detector, *Food Addit. Contam. Part A Chem. Anal. Control Expo. Risk Assess.* 26 (2009) 754–758.
- [8] J.K. Li, R.N. Wu, Q.H. Hu, J.H. Wang, Solid-phase extraction and hplc determination of patulin in apple juice concentrate, *Food Control* 18 (2007) 530–534.
- [9] V. Sewram, J.J. Nair, T.W. Nieuwoudt, N.L. Leggott, G.S. Shephard, Determination of patulin in apple juice by high-performance liquid chromatography-atmospheric pressure chemical ionization mass spectrometry, *J. Chromatogr. A* 897 (2000) 365–374.
- [10] N. Kharandi, M. Babri, J. Azad, A novel method for determination of patulin in apple juices by gc-ms, *Food Chem.* 141 (2013) 1619–1623.
- [11] S. Wu, N. Duan, W. Zhang, S. Zhao, Z. Wang, Screening and development of dna aptamers as capture probes for colorimetric detection of patulin, *Biochem. Anal. Biochem.* 508 (2016) 58–64.
- [12] Y.X. Chen, K.J. Huang, K.X. Niu, Recent advances in signal amplification strategy based on oligonucleotide and nanomaterials for microrna detection-a review, *Biosens. Bioelectron.* 99 (2018) 612–624.
- [13] Y.X. Chen, X. Wu, K.J. Huang, A sandwich-type electrochemical biosensing platform for microrna-21 detection using carbon sphere-mos 2, and catalyzed hairpin assembly for signal amplification, *Sens. Actuators B Chem.* 270 (2018) 179–186.
- [14] Y.H. Wang, K.J. Huang, X. Wu, Recent advances in transition-metal dichalcogenides based electrochemical biosensors: a review, *Biosens. Bioelectron.* 97 (2017) 305–316.
- [15] L. Madianos, G. Tsekenis, E. Skotadis, L. Patsiouras, D. Tsoukalas, A highly sensitive impedimetric aptasensor for the selective detection of acetamiprid and atrazine based on microwires formed by platinum nanoparticles, *Biosens. Bioelectron.* 101 (2018) 268–274.
- [16] B. Zhang, H. Meng, X. Wang, J. Li, H. Chang, W. Wei, Fe³⁺ doped ZnO-Ag photocatalyst for photoelectrochemical sensing platform of ultrasensitive Hg²⁺ detection using exonuclease III-assisted target recycling and DNzyme-catalyzed amplification, *Biosens. Bioelectron.* 255 (2018) 2531–2537.
- [17] R. Jain, A. Thakur, P. Kumar, D. Pooja, Au/ZnO nanocomposites decorated ITO electrodes for voltammetric sensing of selenium in water, *Electrochim. Acta* 290 (2018) 291–302.
- [18] E. Heydari-Bafrooei, M. Amini, M.H. Ardakani, An electrochemical aptasensor based on tio2/mwcnt and a novel synthesized schiff base nanocomposite for the ultrasensitive detection of thrombin, *Biosens. Bioelectron.* 85 (2016) 828–836.
- [19] B. Yuan, J. Zhang, R. Zhang, H. Shi, N. Wang, J. Li, F. Ma, D. Zhang, Cu-based metal-organic framework as a novel sensing platform for the enhanced electro-oxidation of nitrite, *Sens. Actuators B Chem.* 222 (2016) 632–637.
- [20] Y.H. Wang, K.J. Huang, X. Wu, Recent advances in transition-metal dichalcogenides based electrochemical biosensors: a review, *Biosens. Bioelectron.* 100 (2018) 274–281.
- [21] M.H. Ghalehno, M. Mirzaei, M. Torzkadeh-Mahani, Aptamer-based determination of tumor necrosis factor α using a screen-printed graphite electrode modified with gold hexacyanoferrate, *Microchim. Acta* 185 (2018) 165–172.
- [22] M. Kandiah, M.H. Nilsen, S. Usseglio, S. Jakobsen, U. Olsbye, M. Tilset, C. Larabi, E.A. Quadrelli, F. Bonino, K.P. Lillerud, Synthesis and stability of tagged uio-66 zrmofs, *Chem. Mater.* 22 (2010) 6632–6640.
- [23] M. Chen, N. Gan, Y. Zhou, T. Li, Q. Xu, Y. Cao, Y. Chen, A novel aptamer- metal ions- nanoscale MOF based electrochemical biocodes for multiple antibiotics detection and signal amplification, *Sens. Actuators B Chem.* 242 (2017) 1201–1209.
- [24] G. Cai, H.L. Jiang, A modulator-induced defect-formation strategy to hierarchically porous metal-organic frameworks with high stability, *Angew. Chemie* 129 (2017) 578–582.
- [25] S.M. Taghdisi, N.M. Danesh, M.A. Nameghi, M. Ramezani, M. Alibolandi, M. Hassanzadeh-Khayat, A.S. Emrani, K. Abnous, A novel electrochemical aptasensor based on nontarget-induced high accumulation of methylene blue on the surface of electrode for sensing of α -synuclein oligomer, *Biosens. Bioelectron.* 123 (2019) 14–18.
- [26] M. Kandiah, M.H. Nilsen, S. Usseglio, S. Jakobsen, U. Olsbye, M. Tilset, C. Larabi, E.A. Quadrelli, F. Bonino, K.P. Lillerud, Synthesis and stability of tagged uio-66 zrmofs, *Chem. Mater.* 22 (2010) 6632–6640.
- [27] L. Zhu, Y. Li, W. Zeng, Hydrothermal synthesis of hierarchical flower-like zno nanostructure and its enhanced ethanol gas-sensing properties, *Appl. Surf. Sci.* 427 (2018) 281–287.
- [28] W. Raza, M.M. Haque, M. Muneer, J. Apsusc, D. Zno, Synthesis of visible light driven zno: characterization and photocatalytic performance, *Appl. Surfa. Sc.* 322 (2014) 215–224.
- [29] M.M. Hassan, W. Khan, A. Azam, A.H. Naqvi, Influence of cr incorporation on structural, dielectric and optical properties of zno nanoparticles, *J. Ind. Eng. Chem.* 21 (2015) 283–291.
- [30] K.Y.A. Lin, Y.T. Liu, S.Y. Chen, Adsorption of fluoride to uio-66-nh 2 in water: stability, kinetic, isotherm and thermodynamic studies, *J. Colloid Interf. Sci.* 461 (2016) 79–87.
- [31] Y. Jiang, C. Liu, J. Caro, A. Huang, A new UiO-66-NH₂ based mixed-matrix membranes with high CO₂/CH₄ separation performance, *Microporous Mesoporous Mater.* 274 (2019) 203–211.
- [32] B. Rezaei, S. Damiri, Voltammetric behavior of multi-walled carbon nanotubes modified electrode-hexacyanoferrate(II) electrocatalyst system as a sensor for determination of captopril, *Sens. Actuators B Chem.* 134 (2008) 324–331.
- [33] S. Chen, P. Liu, K. Su, Electrochemical aptasensor for thrombin using co-catalysis of hemin/g-quadruplex dnzyme and octahedral cu₂o-au nanocomposites for signal amplification, *Biosens. Bioelectron.* 99 (2017) 338–345.
- [34] W. Zhang, Y. Han, X. Chen, X. Luo, J. Wang, T. Yue, Z. Li, Surface molecularly imprinted polymer capped mn-doped zns quantum dots as a phosphorescent nanosensor for detecting patulin in apple juice, *Food Chem.* 232 (2017) 145–154.
- [35] G. Fang, H. Wang, Y. Yang, G. Liu, S. Wang, Development and application of a quartz crystal microbalance sensor based on molecularly imprinted sol-gel polymer for rapid detection of patulin in foods, *Sens. Actuators B Chem.* 237 (2016) 239–246.